ACS Catalysis

pubs.acs.org/acscatalysis Research Article

A Chemoenzymatic Strategy for Efficient Synthesis of Aporphine Alkaloids

Lu Yang, Yuhan Dai, Lili Sun, Qiqi Wang, Yaxu Ou, Zixin Deng, Xudong Qu,* and Zhi Lin*

Cite This: ACS Catal. 2025, 15, 19918−19925 Read Online

ACCESS | Metrics & More | Article Recommendations | Supporting Information

ABSTRACT: Aporphine alkaloids (APAs) are renowned for their diverse pharmacological activities, but their practical preparation is hindered by challenges, such as poor chiral control and low coupling efficiency, making their production largely dependent on plant extraction. Here, we present a streamlined, modular chemoenzymatic strategy that integrates biocatalysis with photoinduced coupling to efficiently synthesize both natural and unnatural APAs from inexpensive, readily available substrates. This platform employs a sequential enzymatic reaction using engineered imine reductase and cocaine *N*-methyltransferase to convert 2′-halogenated 1-benzyl-dihydroisoquinolines into (*S*)-1-benzyl-tetrahydroisoquinoline precursors, followed by catalyst-free photoinduced coupling to construct diverse APA frameworks. Notably, the highly efficient method enables the gram-scale synthesis of (*S*)-nuciferine in just four steps, demonstrating its practical applicability. By simplifying complex synthesis, enhancing stereoselectivity, and reducing reliance on rare plant sources, this approach offers a powerful platform for APA production and serves as a broadly applicable model for the synthesis of related complex natural products.

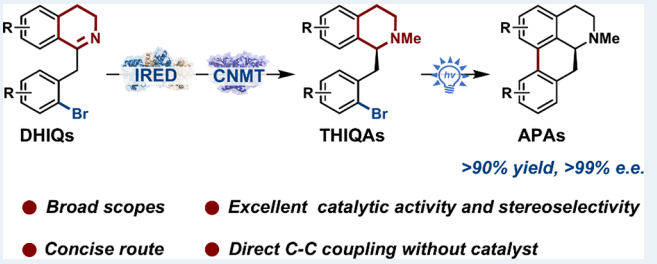

KEYWORDS: *biosynthesis, aporphine alkaloid, imine reductase, catalyst-free photoinduced coupling, chemoenzymatic strategy*

INTRODUCTION

Aporphine alkaloids (APAs) encompass a diverse group of over 500 naturally occurring compounds derived from various plant species.[1] These molecules feature a shared tetracyclic core structure, modified by diverse substituents, oxidation states, and chiral centers, which drive their wide-ranging pharmacological effects, including anticancer, antiviral, antimalarial, anti-inflammatory, lipid-lowering, antiplatelet, and vasodilatory activities (Figure 1A).[1−5] The stereochemistry at C-1 and the substitution pattern on the benzene rings are key determinants of their bioactivity.[6,7] For instance, (*R*)-apomorphine acts as a dopamine receptor agonist and is widely used in the treatment of Parkinson's disease,[8] whereas its enantiomer, (*S*)-apomorphine, functions as an antagonist.[9] Thus, the efficient and precise synthesis of optically pure APAs is critical for unlocking their therapeutic potential. However, commercial APA production currently relies on plant extraction or semisynthesis,[10−14] methods that are vulnerable to environmental disruptions such as disease, pests, and climate variability.[15,16] Furthermore, many APAs are sourced from rare wild plants, limiting their availability and impeding large-scale drug development.

Chemical total synthesis offers an alternative solution to obtain APAs, as demonstrated by Anderson et al., who synthesized (*S*)-glaucine in eight steps using Noyori asymmetric hydrogenation and palladium catalysis (Figure 1B).[17] However, this approach presents several challenges: establishing the C-1 chiral center requires expensive chiral ligands, and the biphenyl formation relies on intramolecular aryl−aryl coupling through palladium catalysis, necessitating high catalyst loads, *N*-protection and deprotection steps, and lengthy synthetic sequences.[14] These factors result in low yields and metal contamination, rendering the large-scale chemical synthesis of APAs impractical. Synthetic biotechnology has emerged as a promising alternative, enabling APA biosynthesis in *Saccharomyces cerevisiae* (Figure 1C). Despite recent progress, this method also faces persistent challenges, including cytotoxicity from heterologous proteins such as norcoclaurine synthase (NCS), intermediate accumulation, narrow enzyme substrate specificity, and the challenge of expressing plant-derived P450 enzymes, such as CYP80G6, which are crucial for biphenyl formation.[18,19] Consequently, the yields remain low—for example, magnoflorine production reaches only 75.8 mg/L—and the approach is restricted to only one or two APA variants, falling short of commercial viability. Thus, achieving an efficient and scalable synthesis of

Received: September 11, 2025
Revised: October 24, 2025
Accepted: November 7, 2025

https://doi.org/10.1021/acscatal.5c06464
ACS Catal. 2025, 15, 19918−19925

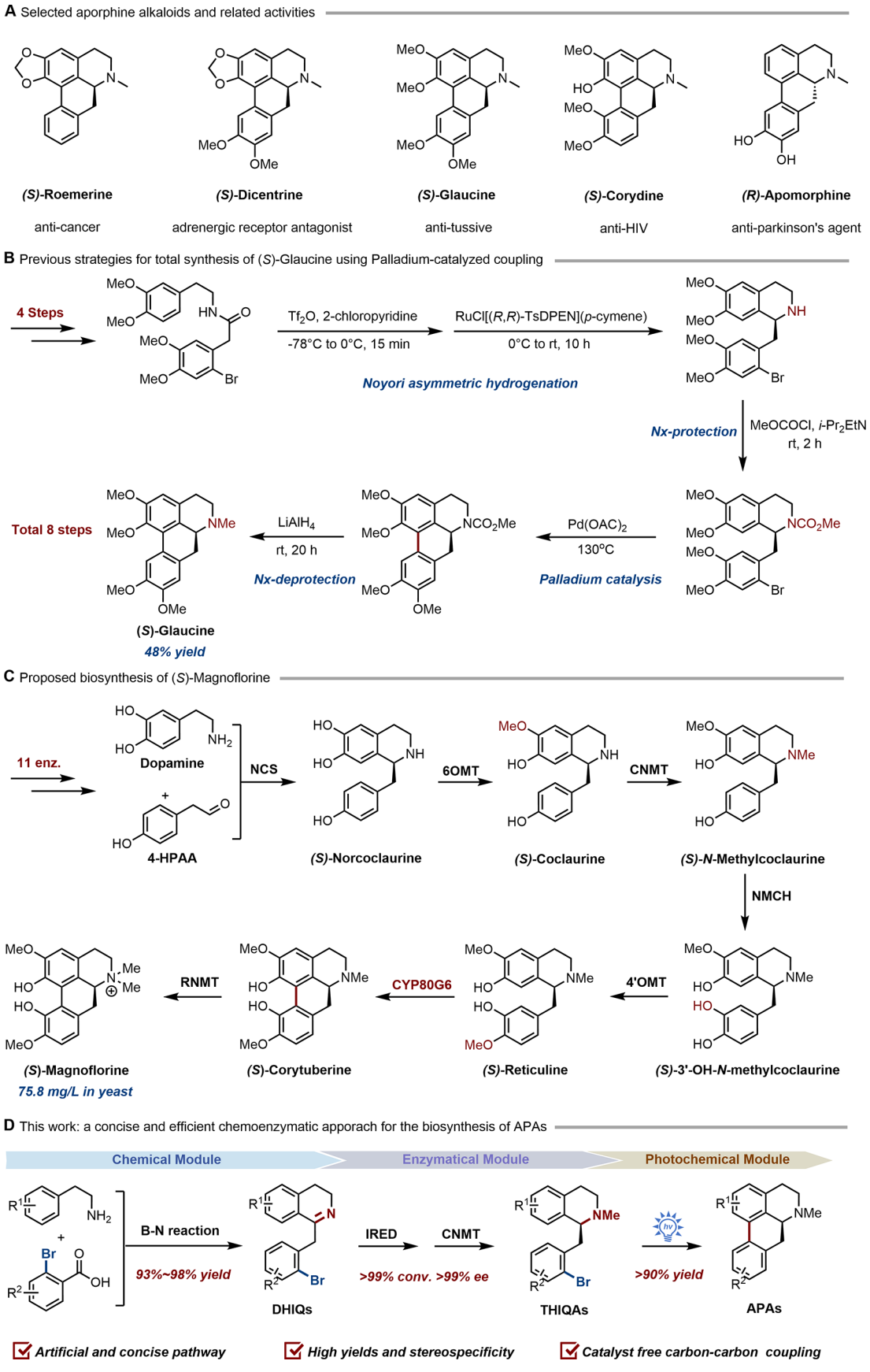

Figure 1. Overview of APAs and their synthetic approaches. (A) Biological and pharmacological properties of some representative APAs. (B) Conventional chemical total synthesis route for APAs. (C) Biosynthetic pathway of (*S*)-Magnoflorine in native plants and heterologous *S. cerevisiae*. (D) Modular chemoenzymatic cascade for the stereoselective synthesis of APAs, developed in this study.

https://doi.org/10.1021/acscatal.5c06464
ACS Catal. 2025, 15, 19918−19925

Scheme 1. Retrosynthetic Analysis of the Aporphines

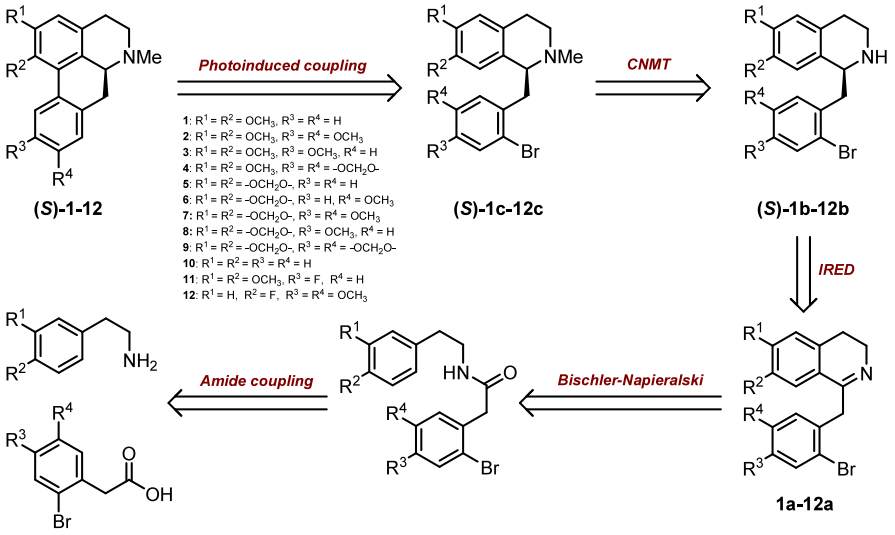

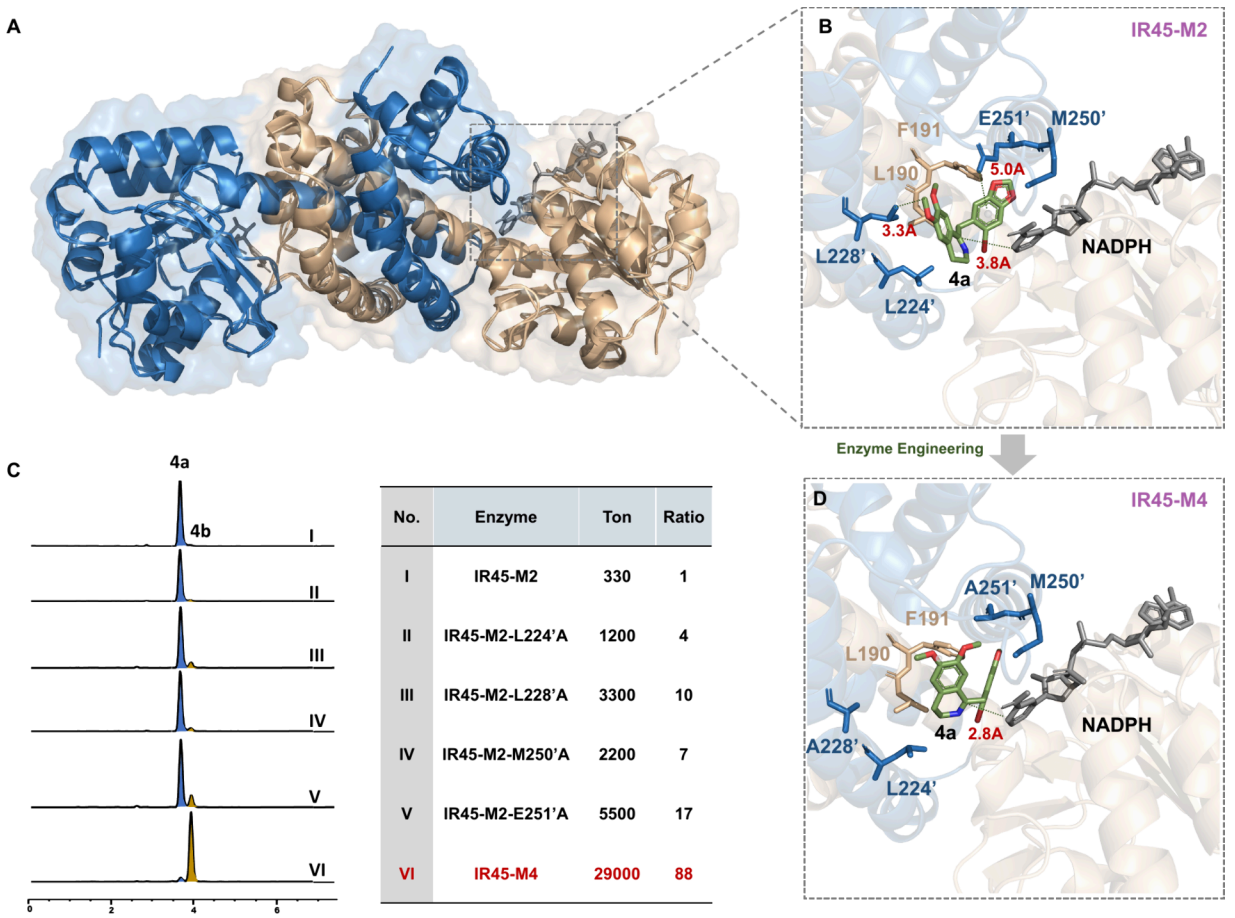

No.	Enzyme	Ton	Ratio
I	IR45-M2	330	1
II	IR45-M2-L224'A	1200	4
III	IR45-M2-L228'A	3300	10
IV	IR45-M2-M250'A	2200	7
V	IR45-M2-E251'A	5500	17
VI	IR45-M4	29000	88

Figure 2. In silico model based on the crystal structure and catalytic activity of mutants. (A) Overall crystal structure of IR45-M2 (PDB: 9J0E). The structure is depicted in cartoon format, with monomers A and B colored in sky blue and wheat, respectively. $NADP^+$ is shown in stick representation and colored in gray, located at the dimer interface. (B) Structure of IR45-M2 docked with 4a (in grass green), with critical residues and distances labeled. (C) Activity of IRED mutants toward 4a. The substrate 4a is represented by the blue peak and the product (*S*)-4b by the wheat peak. Biocatalysis by (I) IR45-M2, (II) IR45-M2-L224'A, (III) IR45-M2-L228'A, (IV) IR45-M2-M250'A, (V) IR45-M2-E251'A, and (VI) IR45-M4. (D) Structure of IR45-M4 docked with 4a (in grass green).

optically pure APAs remains a critical challenge across both chemical and biosynthetic platforms.

Chemoenzymatic strategies, blending synthetic chemistry with biocatalysis, provide a compelling avenue for overcoming these barriers.[20] Building on our previous work on tetrahydroisoquinoline (THIQ) alkaloid synthesis—where we employed an engineered imine reductase (IRED; IR45-M2) to reduce bulky dihydroisoquinoline (DHIQ) precursors to (*S*)-

https://doi.org/10.1021/acscatal.5c06464
ACS Catal. 2025, 15, 19918−19925

products with >99% enantiomeric excess (*e.e.*)—we now introduce a novel modular artificial biosynthesis pathway, comprising the chemical, enzymatical, and photochemical modules for highly enantioselective synthesis of APAs (Figure 1D).[21−23] Integration of a crystal structure-guided, rationally engineered IRED and an *N*-methyltransferase delivered excellent stereocontrol at the challenging molecular core scaffold. Concurrently, optimization of a catalyst-free, photo-induced direct aryl−aryl coupling reaction achieves APA yields of up to 90% with >99% *e.e.* in just four steps. Furthermore, the method is scalable to gram-scale production, providing a practical and sustainable route to pharmaceutically valuable APAs.

RESULTS AND DISCUSSION

Retrosynthetic Analysis and Biocatalytic Transformation of 2′-Halogenated DHIQs by IR45-M2. To address the dual challenges of APA total synthesis—establishing the C-1 chiral center and forming the biphenyl structure—we devised a retrosynthetic strategy that integrates chemical synthesis with biocatalysis (Scheme 1). Organic halides, valued for their accessibility, stability, and ease of activation, are widely used in coupling reactions to form biaryls[24]—a key pharmacophore that enhances protein−target interactions in pharmaceutical design.[25−27] Capitalizing on this, we selected 2′-halogenated 1-benzyl-tetrahydroisoquinolines (1-benzyl-THIQs) as substrates for APA synthesis, bypassing the reliance on the plant-derived P450 enzyme. Drawing on our previous work with IREDs, we intended to employ these enzymes to establish the C-1 chiral center in 2′-halogenated THIQs, starting from 2′-halogenated 1-benzyl-dihydroisoquinolines (1-benzyl-DHIQs) as substrates. This approach overcomes a major limitation of traditional chemical asymmetric catalysis. The 2′-halogenated 1-benzyl-DHIQs could be readily prepared from commercially available phenylethylamine and 2′-halogenated phenylacetic acid through a Bischler−Napieralski reaction, enabling an efficient and streamlined synthetic route.

According to the designed route, we first synthesized 12 2′-Br-1-benzyl-DHIQ precursors (**1a**-**9a**), featuring varied substituents at C6, C7, C3′, and C4′, by optimizing the Bischler−Napieralski reaction with phosphorus pentachloride as dehydrating agents, achieving yields exceeding 90%. However, no IREDs had previously been reported to reduce this compound class. In our previous work, we introduced a biocatalytic method for producing THIQ alkaloids from DHIQ precursors using IREDs and *N*-methyltransferases.[21−23] The engineered IRED IR45-M2 (190L-191F) exhibited excellent substrate tolerance, efficiently reducing a range of bulky benzyl DHIQs to *S*-configuration products with >99% *e.e.*[21,22] Therefore, we evaluated the substrate tolerance of IR45-M2 using compounds **1a**−**9a** and found that IR45-M2 was able to convert all these substrates into *S*-configuration products with high stereoselectivity (>99%). However, the presence of a bromine substituent at the 2′ position significantly impaired the catalytic efficiency of IR45-M2, particularly for **4a**, which exhibited a turnover number of only 330 (Table S1). Kinetic analyses of **1a**, **2a**, and **4a** revealed substantial substrate inhibition, along with low k_{cat} values (Figure S1), indicating the need for targeted engineering of the enzyme's catalytic pocket to enhance performance. This phenomenon presumably originates from nonproductive binding of substrate molecules within the active site at elevated concentrations, generating catalytically inactive complexes. Consequently, targeted engineering of the enzyme's catalytic pocket was necessary to improve performance.

Structural Analysis and Optimization of IR45-M2 for (*S*)-2′-Halogenated 1-Benzyl-THIQs Biosynthesis. To elucidate how IR45-M2 accommodates imine substrates and expands its substrate scope, we resolved its crystal structure in complex with NADP(H) at a resolution of 1.46 Å, which reveals an open conformation. IR45-M2 forms a homodimer with an active site located at the monomer interface (Figure 2A), defined by a cavity comprising residues L190, F191, L224′, L228′, M250′, and E251′ (Figure 2B). Compared to our previous homology model, structural differences were evident in NADP(H) binding and active-site residues, particularly with M250′ and E251′ constricting the pocket, potentially limiting catalysis (Figure S2).

Structural and molecular docking analyses indicated that IR45-M2's poor activity toward **4a** stemmed from (i) spatial restrictions in the binding cavity, where leucines at positions 224′ and 228′ in subunit B displaced the substrate's A-ring; (ii) steric interference from M250′ and E251′, which clashed with **4a**'s methylenedioxy group at a 2.8 Å distance; and (iii) a 3.8 Å gap between **4a**'s C═N bond and NADP(H)'s hydride, misaligning the substrate for reduction. These insights guided the rational engineering of IR45-M2 to enhance its catalytic efficiency.

To alleviate steric hindrance and improve substrate−NADP(H) proximity, we mutated residues L224′, L228′, M250′, and E251′ to alanine, reducing their size. The resulting mutants displayed significantly enhanced activity toward **4a**, with IR45-M2-L228′A and IR45-M2-E251′A showing the most substantial improvements—turnover numbers (TONs) increased by 10-fold and 17-fold, respectively (Figure 2C). Encouraged by these results, we generated the double-mutant IR45-M4 (IR45-M2-L228′A-E251′A), which exhibited an 88-fold activity boost for **4a**. Testing IR45-M4 against the remaining substrates (**1a**-**3a** and **5a**-**9a**) revealed TONs of 2000−30,000—a 1.5- to 15-fold enhancement—while retaining >99% *e.e.* (Figure S3 and Table S1). Notably, substrate inhibition previously observed for compounds **1a**, **2a**, and **4a** was eliminated. Molecular docking confirmed that the mutations expanded the pocket and reduced binding free energy, facilitating a closer NADP(H)−substrate alignment (Figure 2D), therefore significantly enhancing the catalytic efficiency. In addition, we also prepared three engineered substrates (**10a**−**12a**) that either lack a substituent or bear electron-withdrawing substituents on either the A- or C-ring to evaluate the flexibility of IR45-M4. Gratifyingly, all three variants were efficiently reduced, confirming that IR45-M4 tolerates a broad range of electronic substituents (Figure S4).

To assess the preparative potential of IR45-M4, we conducted biotransformations using crude lysate on all 12 imine substrates (**1a**-**12a**) at a 1 mmol scale. Remarkably, the mutant achieved complete substrate conversion within six hours, yielding the corresponding amine products in isolated yields ranging from 91% to 98%, with consistently high enantioselectivity (>99% *e.e.* in all cases, except for **11a** with 93% *e.e.*, Table 1, Figure S4). This performance underscores the robustness of IR45-M4 as a practical catalyst for gram-scale synthesis, consistent with its enhanced activity and alleviated steric constraints demonstrated earlier.

Enzymatic Synthesis of *N*-Methylated and 2′-Halogenated 1-Benzyl-THIQs via Cascade Imine Reduction and *N*-Methylation. Having overcome the key limitations of

https://doi.org/10.1021/acscatal.5c06464
ACS Catal. 2025, 15, 19918−19925

Table 1. Biotransformation of IRED and CNMT[a]

sub.	IR45-M4[b] (yield, *e.e.*)	sub.	CNMT[c] (yield)
1a	97%, >99%	(*S*)-**1b**	96%
2a	98%, >99%	(*S*)-**2b**	97%
3a	95%, >99%	(*S*)-**3b**	98%
4a	96%, >99%	(*S*)-**4b**	96%
5a	93%, >99%	(*S*)-**5b**	94%
6a	93%, >99%	(*S*)-**6b**	93%
7a	96%, >99%	(*S*)-**7b**	95%
8a	94%, >99%	(*S*)-**8b**	96%
9a	95%, >99%	(*S*)-**9b**	95%
10a	92%, >99%	(*S*)-**10b**	97%
11a	95%, 93%	(*S*)-**11b**	96%
12a	91%, >99%	(*S*)-**12b**	94%

[a]All of the stereoselectivity is indicated as (*S*)-configuration. [b]Biotransformation conditions: 100 mM D-glucose, 0.33 μM GDH, 4 mM $NADP^+$, 4 g wet IRED, 50 mM imine substrates, 5% (v/v) DMSO, and potassium phosphate buffer (100 mM, pH 7.0), reactions were conducted at 30 °C, 200 rpm for 6 h. [c]Biotransformation conditions: 5 mM S-adenosyl methionine, 5.81 μM CNMT, 30 mM (*S*)-**1b**-**12b**, 5% (v/v) DMSO, and potassium phosphate buffer (100 mM, pH 7.0), reactions were conducted at 30 °C, 200 rpm for 12 h.

IRED performance, we next established an enzymatic pathway for the synthesis of *N*-methylated and 2'-halogenated 1-benzyl-THIQs. Our previous work demonstrated that cocaine *N*-methyltransferase (CNMT) efficiently converts 1-phenyl-THIQ into its *N*-methylated form. However, its activity toward 2'-halogenated 1-benzyl-THIQs had not yet been tested. We thus evaluated CNMT's performance on substrates (*S*)-**1b**-**12b**, which successfully achieved full conversion to their *N*-methylated products (*S*)-**1c**-**12c** in all instances within 12 h (yielding 94−98%, Table 1, Figure S4). We also evaluated a one-pot method, which also led to product formation. However, due to the differing substrate recognition and catalytic efficiencies of IRED and CNMT, the overall yield was lower compared to the stepwise strategy (data not shown). By surpassing the limitations of traditional chemical approaches, this cascade enzymatic method not only facilitates natural and unnatural THIQs synthesis but also provides a versatile framework for producing other related natural products.

Catalyst-Free Photoinduced C−C Bond Coupling and Its Condition Optimization. To simplify the synthesis of APAs, we first explored the palladium-catalyzed coupling of substrate **1c** without nitrogen protection using an electron-withdrawing group. As anticipated, this approach was unsuccessful, confirming the need for such groups in palladium-based reactions.[28,29] We then investigated a catalyst-free photoinduced coupling method. Previous studies have shown that this approach can directly synthesize APAs, like Bulbocapnine and Steporphine, from 2'-halogenated precursors, albeit with modest yields of 30 and 34%, respectively.[30,31] Despite these limitations, the absence of a catalyst piqued our interest due to its economics and potential to streamline the process.

Using **1c** as a model substrate, we applied a 175 W high-pressure mercury lamp with 3 M HCl under prior established conditions.[11,30] The reaction produced compound **1** with a 15.5% yield after four hours, fully consuming **1c** without notable byproducts. During irradiation, the reaction mixture shifted from a colorless to dark yellow. Notably, commercially sourced **1**, initially pale yellow, also darkened upon prolonged air exposure, suggesting that **1** may be susceptible to oxidation under light, resulting in low yield. Thus, the reaction was conducted under a nitrogen atmosphere. To our delight, this

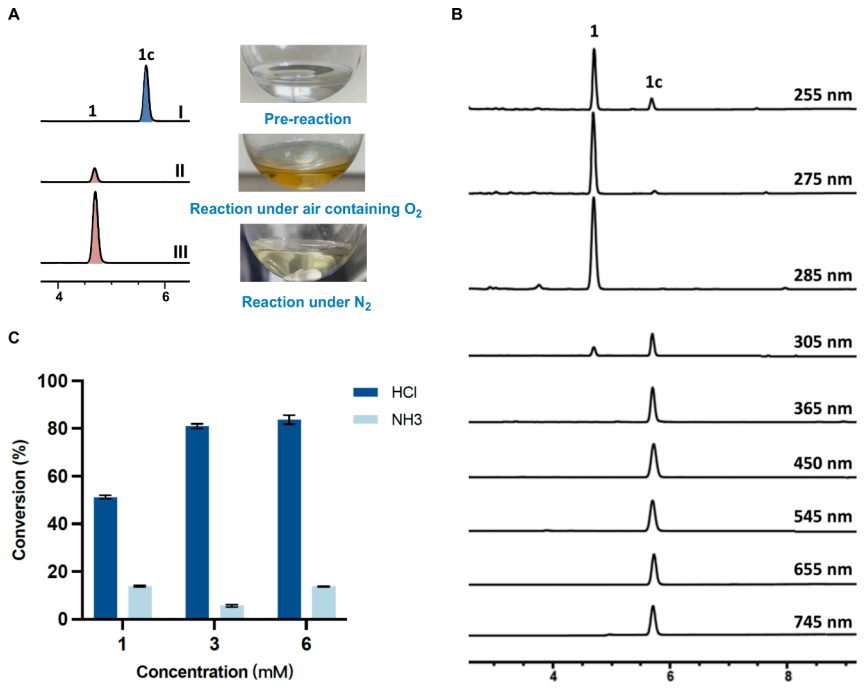

Figure 3. Optimization of reaction conditions for catalyst-free photoinduced coupling. (A) Effect of gas factors on the photoinduced reactions. The conversion of 1c was measured under N_2 or O_2 for 4 h, respectively. The substrate 1c is indicated by the blue peak; the product 1 is indicated by the pink peak. (I) Pre-reaction; (II) reaction under air containing O_2; and (III) reaction under N_2. (B) HPLC analysis of photoinduced reactions of 1c at different wavelengths. Detection of 1c (5 mM) conversion at nine different wavelengths for 30 min. (C) Comparison of coupling rates of 1c under different concentrations of HCl and NH_3. The conversion rate of 1c (5 mM) was measured after 10 min at 285 nm.

https://doi.org/10.1021/acscatal.5c06464
ACS Catal. 2025, 15, 19918−19925

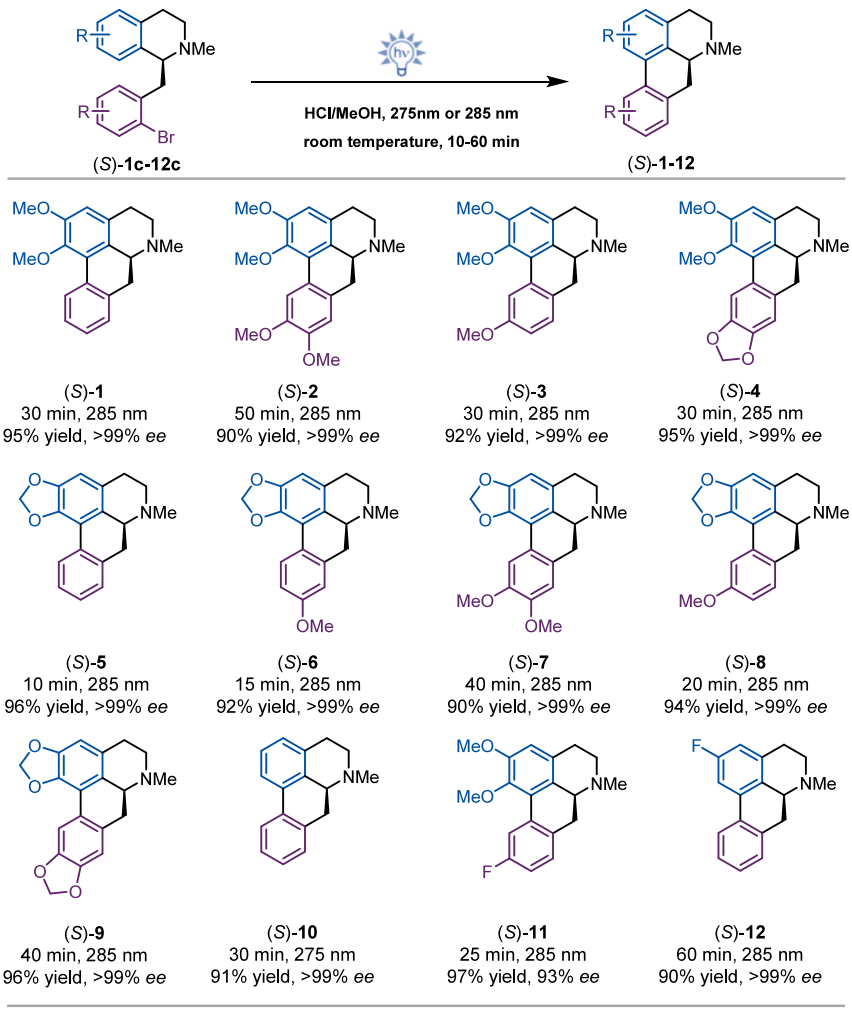

Figure 4. Evaluation of the photoinduced coupling substrate scope. Reaction conditions: 0.03 mol (*S*)-1c-12c, 3 M HCl, 10 W LED, 10−60 min. The reaction time was determined by complete consumption of the substrate.

change markedly improved the conversion of **1c** from 15.5% to 97% (based on the HPLC peak area, Figure 3A).

Catalyst-free photoinduced coupling of aryl halides with aryl groups to form APAs has been documented, however, typically yielding low-to-moderate results accompanied by unproven mechanisms.[32−34] To further explore the factors influencing coupling efficiency, we switched a high-pressure mercury lamp to a multichannel LED photoreactor, which minimized thermal effects and allowed precise wavelength control. Testing nine wavelengths (250−745 nm) at 10 W power revealed optimal coupling below 300 nm, peaking at ∼285 nm with 99% conversion of **1c** in 30 min (Figure 3B), which was consistent with the maximum absorption of **1c** (283 nm).

According to the literature,[35,36] the light can induce base (such as NH_3 and DMA) to donate an electron to aromatic halide to form a radical anion, followed by heterolytic cleavage of aryl−halogen bond, accompanied by the departure of the halogen anion. However, the THIQ precursors containing basic nitrogen (such as NH or NMe) either failed to produce cyclized products or gave aporphines in low yield.[36] Therefore, we explored and optimized the acid−base concentration conditions. The reaction rate decreased with lower HCl concentrations or when it was replaced by NH_3 (Figure 3C). We speculate that protons accelerate the dissociation of bromide; consequently, elevated acid concentrations facilitate the reaction.

Substrate Scope and Scalability. To evaluate the substrate scope of this photoinduced C−C bond coupling reaction, we tested the remaining 11 compounds with diverse substituents, yielding the corresponding products efficiently (90−97% yield, Figure 4), confirming that the transformation tolerates broad electronic substituents and that substitution on the aromatic ring is not obligatory for reactivity.

Finally, a preparative-scale reaction was conducted by using **1a** as the model substrate. By optimizing the ratios of $NADP^+$, GDH, and IR45-M4, coupling this enzymatic step with chemical methylation and a photoinduced reaction, we achieved gram-scale production of (*S*)-**1b**. Integrating this enzymatic step with chemical methylation and photoinduced coupling, we obtained 1.05 g of (*S*)-**1** with an overall yield of up to 83% and an *e.e.* of >99% (Figure 5), demonstrating the practical utility of this approach.

CONCLUSION

APAs are a valuable class of pharmaceutical compounds, but their commercial production is limited by the difficulty of sourcing them from rare wild plants and the complexity of enantioselectively constructing their tetracyclic scaffolds. Traditional synthetic strategies often involve extensive

https://doi.org/10.1021/acscatal.5c06464
ACS Catal. 2025, 15, 19918−19925

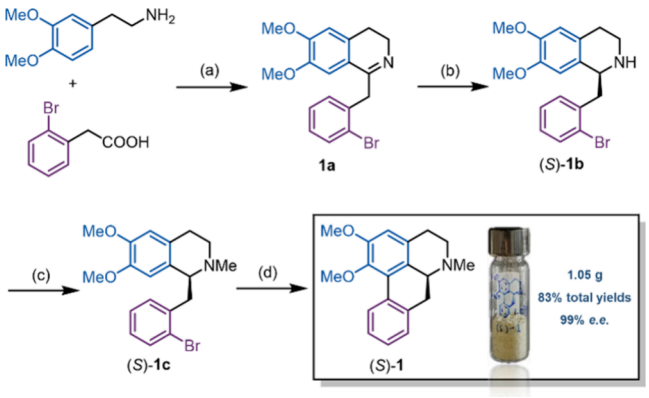

Figure 5. Gram-scale synthesis of (*S*)-1. Reagents and conditions: (a) EDCI/HOBt (1.1 equiv), TEA (3 equiv), CH_2Cl_2, 0 °C → rt, 6 h; PCl_5 (2 equiv), CH_2Cl_2, 0 °C → rt, 6 h, 98%. (b) IR45-M4, potassium phosphate buffer (0.1 M, pH 7.0), 30 °C, 6 h, 95%. (c) 37% HCHO (10 equiv), $NaBH_4$ (2 equiv), MeOH, rt, 8 h, 97%. (d) HCl (3 M), 285 nm LED, MeOH, rt, N_2, 92%.

protecting group manipulations and palladium-catalyzed couplings, making the process laborious and inefficient. To address these challenges, we developed a modular chemoenzymatic strategy by integrating a photoinduced coupling reaction with an IRED-based biocatalysis.

Through crystal structure-guided protein engineering, we significantly enhanced the substrate tolerance of IR45 toward 2'-halogenated 1-benzyl-THIQs compounds. The engineered variant, IR45-M4, exhibited improved steric hindrance tolerance, enabling the synthesis of both natural and unnatural THIQs. Meanwhile, the light-activated, catalyst-free C−C coupling reaction greatly simplified the synthetic route, boosting yields and enhancing the enantiomeric purity, thereby enabling the efficient production of APAs.

This artificial biosynthesis strategy not only streamlined the synthesis but also improved yields and enantiomeric excess, enabling cost-effective production of these medicinally significant compounds. For example, the cost of isolating compound **1** from plants exceeds $6500 per kilogram, whereas the raw materials for the synthetic route reported here cost less than $400. In summary, this modular chemoenzymatic approach not only advances APA synthesis but also establishes a sustainable and efficient C−C bond formation strategy with broad applications in both pharmaceutical manufacturing and material sciences.

METHODS

All information describing experimental details and containing the data used for determination of the structures of all new compounds can be found in the Supporting Information.

ASSOCIATED CONTENT

Supporting Information

The Supporting Information is available free of charge at https://pubs.acs.org/doi/10.1021/acscatal.5c06464.

Full experimental methods, plasmids, and strains used in this study, characterization data, X-ray structures of protein and compounds, HPLC analysis (PDF)

Crystallographic data of **2b**, **4b**, **5b**, **7b**, and **9b** (CIF) (ZIP)

AUTHOR INFORMATION

Corresponding Authors

Xudong Qu − *State Key Laboratory of Microbial Metabolism & School of Life Sciences and Biotechnology, Shanghai Jiao Tong University, Shanghai 200240, China; Zhangjiang Institute for Advanced Study, Shanghai Jiao Tong University, Shanghai 201203, China;* orcid.org/0000-0002-3301-8536; Email: quxd19@sjtu.edu.cn

Zhi Lin − *State Key Laboratory of Microbial Metabolism & School of Life Sciences and Biotechnology, Shanghai Jiao Tong University, Shanghai 200240, China; Zhangjiang Institute for Advanced Study, Shanghai Jiao Tong University, Shanghai 201203, China;* orcid.org/0009-0005-2240-449X; Email: linz@sjtu.edu.cn

Authors

Lu Yang − *State Key Laboratory of Microbial Metabolism & School of Life Sciences and Biotechnology, Shanghai Jiao Tong University, Shanghai 200240, China; Zhangjiang Institute for Advanced Study, Shanghai Jiao Tong University, Shanghai 201203, China*

Yuhan Dai − *State Key Laboratory of Microbial Metabolism & School of Life Sciences and Biotechnology, Shanghai Jiao Tong University, Shanghai 200240, China; Zhangjiang Institute for Advanced Study, Shanghai Jiao Tong University, Shanghai 201203, China*

Lili Sun − *State Key Laboratory of Microbial Metabolism & School of Life Sciences and Biotechnology, Shanghai Jiao Tong University, Shanghai 200240, China; Zhangjiang Institute for Advanced Study, Shanghai Jiao Tong University, Shanghai 201203, China*

Qiqi Wang − *State Key Laboratory of Microbial Metabolism & School of Life Sciences and Biotechnology, Shanghai Jiao Tong University, Shanghai 200240, China; Zhangjiang Institute for Advanced Study, Shanghai Jiao Tong University, Shanghai 201203, China*

Yaxu Ou − *State Key Laboratory of Microbial Metabolism & School of Life Sciences and Biotechnology, Shanghai Jiao Tong University, Shanghai 200240, China*

Zixin Deng − *State Key Laboratory of Microbial Metabolism & School of Life Sciences and Biotechnology, Shanghai Jiao Tong University, Shanghai 200240, China*

Complete contact information is available at: https://pubs.acs.org/10.1021/acscatal.5c06464

Notes

The authors declare no competing financial interest.

ACKNOWLEDGMENTS

We thank Dr. Jian Li for the help in substrate synthesis; the staff of beamline 10U2 at the Shanghai Synchrotron Radiation Facility. This work was supported in part by the NSFC (22377074 and 22107069 to Z.L., 32425033 to X.Q.), the National Key R&D Program of China (2021YFC2100600 to Z.L., 2025YFA0921000 to X.Q.), and the Key Project for Synthetic Biology of Shanghai (24HC2810800 to Z.L.).

REFERENCES

(1) Guinaudeau, H.; Lebœuf, M.; Cavé, A. Aporphinoid alkaloids. *J. Nat. Prod.* **1994**, *57*, 1033−1135.

(2) Chen, K. S.; Ko, F. N.; Teng, C. M.; Wu, Y. C. Antiplatelet and vasorelaxing actions of some aporphinoids. *Planta. Med.* **1996**, *62*, 133−136.

(3) Guo, Y.; Ding, Y.; Wu, G.; Zhu, S.; Sun, Y.; Yan, S.; Qian, F.; Jin, H.; Zhang, W. Three new alkaloids from Xylopia vielana and their antiinflammatory activities. *Fitoterapia* **2018**, *127*, 96−100.
(4) Qing, Z.; Huang, J.; Yang, X.; Liu, J.; Cao, H.; Xiang, F.; Cheng, P.; Zeng, J. Anticancer and reversing multidrug resistance activities of natural isoquinoline alkaloids and their structure-activity relationship. *Curr. med. chem.* **2019**, *25*, 5088−5114.
(5) Mohamed, S. M.; Hassan, E. M.; Ibrahim, N. A. Cytotoxic and antiviral activities of aporphine alkaloids of Magnolia grandiflora L. *Nat. Prod. Res.* **2010**, *24*, 1395−1402.
(6) Agbo, F.; Isaacson, S. H.; Gil, R.; Chiu, Y.-Y.; Brantley, S. J.; Bhargava, P.; Navia, B. Pharmacokinetics and comparative bioavailability of apomorphine sublingual film and subcutaneous apomorphine formulations in patients with Parkinson's disease and "OFF" episodes: results of a randomized, three-way crossover, open-label study. *Neurol. Ther.* **2021**, *10* (2), 693−709.
(7) Kang, H.; Jang, S. W.; Pak, J. H.; Shim, S. Glaucine inhibits breast cancer cell migration and invasion by inhibiting MMP-9 gene expression through the suppression of NF-kappaB activation. *Mol. Cell. Biochem.* **2015**, *403* (1−2), 85−94.
(8) Merello, M.; Pikielny, R.; Cammarota, A.; Leiguarda, R. Comparison of subcutaneous apomorphine versus dispersible madopar latency and effect duration in Parkinson's disease patients: a double-blind single-dose study. *Clin. Neuropharmacol.* **1997**, *20*, 165−167.
(9) Goldman, M. E.; Kebabian, J. W. Apomorphine enantiomers. Interactions with D-1 and D-2 dopamine receptors. *Mol. Pharmacol. Mol. Pharmacol.* **1984**, *25* (1), 18−23.
(10) Udvardy, A.; Sipos, A. Salutaridine and its derivatives as thebaine-equivalents in the synthesis of aporphines. *Open Chem.* **2013**, *11* (12), 2022−2030.
(11) Hoshino, O. Recent developments on the synthesis of aporphine alkaloids. *Studies in Nat. Prod. Chem.* **1995**, *16*, 503−546.
(12) Chrzanowska, M.; Grajewska, A.; Rozwadowska, M. D. Asymmetric synthesis of isoquinoline alkaloids: 2004−2015. *Chem. Rev.* **2016**, *116* (19), 12369−12465.
(13) Perecim, G. P.; Deflon, V. M.; Martins, G. R.; Pinto, L. M. C.; Casagrande, G. A.; Oliveira-Silva, D.; Raminelli, C. Stereoselective total synthesis of (*S*)- and (*R*)-nuciferine using benzyne chemistry. *Tetrahedron* **2020**, *76* (38), No. 131461.
(14) Lafrance, M.; Blaquiere, N.; Fagnou, K. Direct intramolecular arylation of unactivated arenes: application to the synthesis of aporphine alkaloids. *Chem. Commun.* **2004**, *24*, 2874−2875.
(15) Sun, S.; Wei, Y.; Wang, H.; Tang, L.; Deng, B. Simultaneous electrochemiluminescence determination of sinomenine, cepharanthine and tetrahydropalmatine in *Stephania epigaea* by capillary electrophoresis coupled with ultrasonic-assisted aqueous two-phase extraction. *Int. J. Electrochem. Sci.* **2020**, *15* (6), 5002−5017.
(16) Tarabasz, D.; Kukula-Koch, W. Palmatine: A review of pharmacological properties and pharmacokinetics. *Phytother. Res.* **2020**, *34* (1), 33−50.
(17) Pieper, P.; Mchugh, E.; Amaral, M.; Tempone, A. G.; Anderson, E. A. Enantioselective synthesis and anti-parasitic properties of aporphine natural products. *Tetrahedron* **2020**, *76* (2), No. 130814.
(18) Li, Q.; Jiao, X.; Li, X.; Shi, W.; Ma, Y.; Tan, X.; Gan, J.; Liu, J.; Yang, J.; Wang, J.; Jin, B.; Chen, T.; Su, P.; Zhao, Y.; Zhang, Y.; Tang, J.; Cui, G.; Chen, Y.; Guo, J.; Huang, L. Identification of the cytochrome P450s responsible for the biosynthesis of two types of aporphine alkaloids and their de novo biosynthesis in yeast. *J. Integr. Plant. Biol.* **2024**, *66* (8), 1703−1717.
(19) Ikezawa, N.; Iwasa, K.; Sato, F. Molecular cloning and characterization of CYP80G2, a cytochrome P450 that catalyzes an intramolecular C-C phenol coupling of (*S*)-reticuline in magnoflorine biosynthesis, from cultured *Coptis japonica* cells. *J. Biol. Chem.* **2008**, *283* (14), 8810−8821.
(20) Roddan, R.; Carter, E. M.; Thair, B.; Hailes, H. C. Chemoenzymatic approaches to plant natural product inspired compounds. *Nat. Prod. Rep.* **2022**, *39* (7), 1375−1382.
(21) Zhu, J.; Tan, H.; Yang, L.; Dai, Z.; Zhu, L.; Ma, H.; Deng, Z.; Tian, Z.; Qu, X. Enantioselective synthesis of 1-aryl-substituted tetrahydroisoquinolines employing imine reductase. *ACS Catal.* **2017**, *7*, 7003−7007.
(22) Yang, L.; Zhu, J.; Sun, C.; Deng, Z.; Qu, X. Biosynthesis of plant tetrahydroisoquinoline alkaloids through an imine reductase route. *Chem. Sci.* **2020**, *11*, 364−371.
(23) Zhu, J.; Yang, L.; Wu, J.; Deng, Z.; Qu, X. Engineering imine reductase for efficient biosynthesis of 1-aryl-tetrahydro-β-carbolines and their n-methylation products. *ACS Catal.* **2022**, *12*, 9823−9830.
(24) Petrone, D. A.; Ye, J.; Lautens, M. Modern transition-metal-catalyzed carbon-halogen bond formation. *Chem. Rev.* **2016**, *116* (39), 8003−8104.
(25) Hajduk, P. J.; Bures, M.; Praestgaard, J.; Fesik, S. W. Privileged molecules for protein binding identified from NMR-based screening. *J. Med. Chem.* **2000**, *43*, 3443−3447.
(26) Bringmann, G.; Günther, C.; Ochse, M.; Schupp, O.; Tasler, S. Biaryls in Nature: A Multi-Facetted Class of Stereochemically, Biosynthetically, and Pharmacologically Intriguing Secondary Metab-olites. In *Progress in the Chemistry of Organic Natural Products*; Herz, W.; Falk, H.; Kirby, G. W.; Moore, R. E., Eds.; Springer: Vienna, 2001; Vol. *82*, pp 1−249.
(27) Horton, D. A.; Bourne, G. T.; Smythe, M. L. The combinatorial synthesis of bicyclic privileged structures or privileged substructures. *Chem. Rev.* **2003**, *103*, 893−930.
(28) Zhong, M.; Jiang, Y.; Chen, Y.; Yan, Q.; Liu, J.; Di, D. Asymmetric total synthesis of (*S*)-isocorydine. *Tetrahedron: Asymmetry* **2015**, *26*, 1145−1149.
(29) Hellal, M.; Singh, S.; Cuny, G. D. Monoligated Pd(0)-catalyzed intramolecular ortho- and para-arylation of phenols for the synthesis of aporphine alkaloids. Synthesis of (−)-lirinine. *Tetrahedron* **2012**, *68* (6), 1674−1681.
(30) Soicke, H.; Hassan, G. A.; Frenzel, U.; Görler, K. Versuche zur photochemischen Synthese von Bulbocapnin. *Archiv. der. Pharmazie.* **1988**, *321*, 149−152.
(31) Doshi, H.; Cardis, A. B.; Crelling, J. K.; Miller, S. I.; Dalton, D. R.; Zacharias, D. E.; Glusker, J. P. Hofmann degradation of β-hydroxy ammonium salts. II. 4-hydroxybenzylisoquinolines and 4-hydroxyaporphines. *J. Org. Chem.* **1987**, *52*, 2604−2608.
(32) Grimshaw, J.; de Silva, A. P. Photochemistry and photocyclization of aryl halides. *Chem. Soc. Rev.* **1981**, *10* (2), 181.
(33) Kupchan, S. M.; Kanojia, R. M. Photochemical synthesis of aporphines. *Tetrahedron lett* **1966**, *7* (44), 5353−5356.
(34) Cava, M. P.; Mitchell, M. J.; Havlicek, S. C.; Lindert, A.; Spangler, R. J. Photochemical routes to aporphines. New syntheses of nuciferine and glaucine. *J. Org. Chem.* **1970**, *35* (1), 175−179.
(35) Grodowski, M.; Latowski, T. A study on a photochemical reaction in the system N, N-dimethylaniline-bromobenzene. *Tetrahedron* **1974**, *30* (6), 767−772.
(36) Barolo, S. M.; Teng, X.; Cuny, G. D.; Rossi, R. A. Syntheses of aporphine and homoaporphine alkaloids by intramolecular-arylation of phenols with aryl halides via S1 reactions in liquid ammonia. *J. Org. Chem.* **2006**, *71* (22), 8493−8499.

https://doi.org/10.1021/acscatal.5c06464
ACS Catal. 2025, 15, 19918−19925